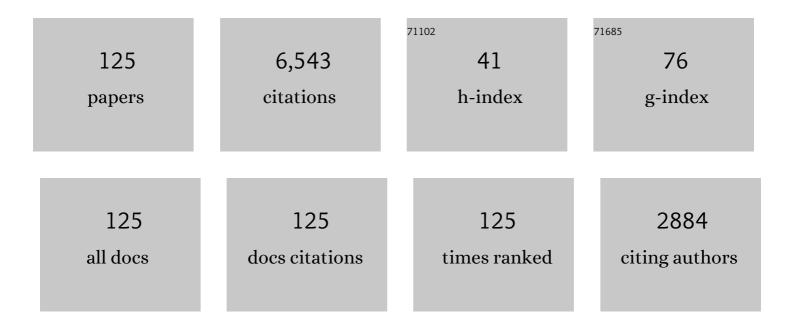
List of Publications by Year in descending order

Source: https://exaly.com/author-pdf/6007516/publications.pdf Version: 2024-02-01



#	Article	IF	CITATIONS
1	Stress Corrosion Susceptibility and Electrochemical Characteristic of X80 Under a Disbonded Coating in a Low-pH Soil Solution with Cathodic Protection. Journal of Materials Engineering and Performance, 2022, 31, 2102-2111.	2.5	2
2	Caustic corrosion cracking of the octene tube in the fertilizer industry. Engineering Failure Analysis, 2022, 133, 105953.	4.0	3
3	Stress corrosion cracking behavior of high-strength mooring-chain steel in the SO2-polluted coastal atmosphere. International Journal of Minerals, Metallurgy and Materials, 2022, 29, 1186-1196.	4.9	2
4	Effect of cathodic potential on stress corrosion cracking behavior of 21Cr2NiMo steel in simulated seawater. International Journal of Minerals, Metallurgy and Materials, 2022, 29, 263-270.	4.9	1
5	Extracellular electron transfer routes in microbiologically influenced corrosion of X80 steel by Bacillus licheniformis. Bioelectrochemistry, 2022, 145, 108074.	4.6	7
6	Corrosion and tribocorrosion behaviors of ternary TiZrN coating on 304 stainless steel prepared by HiPIMS. Materials Today Communications, 2022, 31, 103258.	1.9	1
7	Effect of Hydrogen Charging on the Stress Corrosion Cracking Behavior of X70 Steel in Simulated Deep Seawater Environment. Metals, 2022, 12, 334.	2.3	9
8	Initiation Mechanism of Localized Corrosion Induced by Al2O3-MnS Composite Inclusion in Low-Alloy Structural Steel. Metals, 2022, 12, 587.	2.3	7
9	Electrochemical studies of microbiologically influenced corrosion of X80 steel by nitrate-reducing Bacillus licheniformis under anaerobic conditions. Journal of Materials Science and Technology, 2022, 118, 208-217.	10.7	15
10	Nitrate-reducing-bacteriaÂassisted hydrogen embrittlement of X80 steel in a near-neutral pH solution. Corrosion Science, 2022, 202, 110317.	6.6	4
11	Corrosion behavior of typical hot rolled sheets in humid storage environments. Anti-Corrosion Methods and Materials, 2022, ahead-of-print, .	1.5	0
12	Study of biofilm-influenced corrosion on X80 pipeline steel by a nitrate-reducing bacterium, Bacillus cereus, in artificial Beijing soil. Colloids and Surfaces B: Biointerfaces, 2021, 197, 111356.	5.0	27
13	Accelerating effect of catalase on microbiologically influenced corrosion of 304 stainless steel by the halophilic archaeon Natronorubrum tibetense. Corrosion Science, 2021, 178, 109057.	6.6	26
14	Recent advances on environmental corrosion behavior and mechanism of high-entropy alloys. Journal of Materials Science and Technology, 2021, 80, 217-233.	10.7	250
15	Effect of cathodic polarisation on stress corrosion cracking behaviour of a Ni(Fe, Al)-maraging steel in artificial seawater. Corrosion Science, 2021, 179, 109176.	6.6	33
16	Effect of Tempering Temperature on the Microstructure and Stress Corrosion Cracing Susceptibility of Ultra-High-Strength Mooring Steel. Journal of Materials Engineering and Performance, 2021, 30, 4217-4229.	2.5	2
17	Comparison of microbiologically influenced corrosion of structural steel by nitrate-reducing bacteria in aerobic and anaerobic conditions. Construction and Building Materials, 2021, 288, 123091.	7.2	4
18	Fundamental understanding on the effect of Cr on corrosion resistance of weathering steel in simulated tropical marine atmosphere. Corrosion Science, 2021, 186, 109427.	6.6	91

#	Article	IF	CITATIONS
19	Analysis of Corrosion Evolution in Carbon Steel in the Subtropical Atmospheric Environment of Sichuan. Journal of Materials Engineering and Performance, 2021, 30, 8014-8022.	2.5	15
20	Distinct beneficial effect of Sn on the corrosion resistance of Cr–Mo low alloy steel. Journal of Materials Science and Technology, 2021, 81, 175-189.	10.7	39
21	Influence of NaCl concentration on microbiologically influenced corrosion of carbon steel by halophilic archaeon Natronorubrum tibetense. Bioelectrochemistry, 2021, 140, 107746.	4.6	14
22	The corrosion behavior and film properties of Al-containing high-entropy alloys in acidic solutions. Applied Surface Science, 2021, 560, 149854.	6.1	58
23	The influence of temperature and dissolved oxygen on the electrochemical nature of Al–Zn–In–Ga galvanic anode. Surface Topography: Metrology and Properties, 2021, 9, 035054.	1.6	1
24	Microstructure and mechanical properties of FeCoCrNiMo0.1 high-entropy alloy with various annealing treatments. Materials Characterization, 2021, 179, 111313.	4.4	13
25	Stress corrosion mechanism and susceptibility of X80 steel under a disbonded coating in an acidic soil solution. Journal of Materials Research and Technology, 2021, 14, 533-547.	5.8	7
26	Evolution in microstructure, wear, corrosion, and tribocorrosion behavior of Mo-containing high-entropy alloy coatings fabricated by laser cladding. Corrosion Science, 2021, 191, 109727.	6.6	77
27	Optimization of Mo on the corrosion resistance of Cr-advanced weathering steel designed for tropical marine atmosphere. Construction and Building Materials, 2021, 302, 124346.	7.2	30
28	Corrosion mechanism of nitrate reducing bacteria on X80 steel correlated to its intermediate metabolite nitrite. Construction and Building Materials, 2021, 303, 124454.	7.2	12
29	Fundamental understanding on the microstructure and corrosion resistance of Cr-(Cr, Al)2O3 composite coatings in-situ synthetized by reactive plasma spraying. Surface and Coatings Technology, 2021, 423, 127608.	4.8	5
30	Microstructure and corrosion resistance of duplex coatings deposited on TC17 alloys by MAO and HiPIMS. Materials Letters, 2021, 303, 130506.	2.6	5
31	Exploration of the processing scheme of a novel Ni(Fe, Al)-maraging steel. Journal of Materials Research and Technology, 2021, 10, 225-239.	5.8	7
32	X-ray photoelectron spectroscopy and electrochemical investigation of the passive behavior of high-entropy FeCoCrNiMox alloys in sulfuric acid. Applied Surface Science, 2020, 499, 143903.	6.1	89
33	Influence of carbon on the corrosion behaviour of interstitial equiatomic CoCrFeMnNi high-entropy alloys in a chlorinated concrete solution. Corrosion Science, 2020, 163, 108287.	6.6	123
34	Microbiologically influenced corrosion of 304 stainless steel by halophilic archaea Natronorubrum tibetense. Journal of Materials Science and Technology, 2020, 46, 12-20.	10.7	20
35	1Influence of graphene oxide additive on the tribological and electrochemical corrosion properties of a PEO coating prepared on AZ31 magnesium alloy. Tribology International, 2020, 146, 106135.	5.9	71
36	Microbiologically influenced corrosion of FeCoCrNiMo0.1 high-entropy alloys by marine Pseudomonas aeruginosa. Corrosion Science, 2020, 165, 108390.	6.6	67

#	Article	IF	CITATIONS
37	The AC corrosion and SCC mechanism of X80 pipeline steel in near-neutral pH solution. Engineering Failure Analysis, 2020, 118, 104904.	4.0	15
38	The influence of half-cycle rectified sinusoidal alternating current (AC) on corrosion of X80 pipeline steel in an acid bicarbonate solution. Anti-Corrosion Methods and Materials, 2020, 67, 248-254.	1.5	2
39	Characteristics of hydrogen embrittlement in high-pH stress corrosion cracking of X100 pipeline steel in carbonate/ bicarbonate solution. Construction and Building Materials, 2020, 263, 120124.	7.2	38
40	Stress Corrosion Cracking of 2205 Duplex Stainless Steel with Simulated Welding Microstructures in Simulated Sea Environment at Different Depths. Journal of Materials Engineering and Performance, 2020, 29, 5476-5489.	2.5	11
41	Revealing bioinorganic interface in microbiologically influenced corrosion with FIB-SEM/TEM. Corrosion Science, 2020, 173, 108763.	6.6	15
42	Evidencing the uptake of electrons from X80 steel by Bacillus licheniformis with redox probe, 5-cyano-2,3-ditolyl tetrazolium chloride. Corrosion Science, 2020, 168, 108569.	6.6	20
43	The study of microbiologically influenced corrosion of 2205 duplex stainless steel based on high-resolution characterization. Corrosion Science, 2020, 174, 108842.	6.6	35
44	Failure analysis of a 304 stainless steel heat exchanger in liquid sulfur recovery units. Engineering Failure Analysis, 2020, 116, 104729.	4.0	24
45	Comparative study of the stress corrosion behavior of a multiuse bainite steel in the simulated tropical marine atmosphere and seawater environments. Construction and Building Materials, 2020, 239, 117903.	7.2	46
46	Effect of molybdenum content on the microstructure and corrosion behavior of FeCoCrNiMox high-entropy alloys. Journal of Materials Science and Technology, 2020, 46, 64-73.	10.7	138
47	Microbiologically influenced corrosion of 304 stainless steel by nitrate reducing Bacillus cereus in simulated Beijing soil solution. Bioelectrochemistry, 2020, 133, 107477.	4.6	25
48	Comparative study on corrosion fatigue behaviour of high strength low alloy steel and simulated HAZ microstructures in a simulated marine atmosphere. International Journal of Fatigue, 2020, 137, 105666.	5.7	30
49	Local chemistry–electrochemistry and stress corrosion susceptibility of X80 steel below disbonded coating in acidic soil environment under cathodic protection. Construction and Building Materials, 2020, 243, 118203.	7.2	33
50	Microbiologically influenced corrosion of X80 pipeline steel by nitrate reducing bacteria in artificial Beijing soil. Bioelectrochemistry, 2020, 135, 107551.	4.6	22
51	Stress-assisted microbiologically influenced corrosion mechanism of 2205 duplex stainless steel caused by sulfate-reducing bacteria. Corrosion Science, 2020, 173, 108746.	6.6	74
52	Effect of AC Current Density on the Stress Corrosion Cracking Behavior and Mechanism of E690 High-Strength Steel in Simulated Seawater. Journal of Materials Engineering and Performance, 2019, 28, 6931-6941.	2.5	11
53	Effect of alternating current and Bacillus cereus on the stress corrosion behavior and mechanism of X80 steel in a Beijing soil solution. Bioelectrochemistry, 2019, 127, 49-58.	4.6	22
54	Electrochemical characteristic and stress corrosion behavior of API X70 high-strength pipeline steel under a simulated disbonded coating in an artificial seawater environment. Journal of Electroanalytical Chemistry, 2019, 845, 92-105.	3.8	29

#	Article	IF	CITATIONS
55	Interaction between hydrogen and cyclic stress and its role in fatigue damage mechanism. Corrosion Science, 2019, 157, 146-156.	6.6	34
56	Effect of pre-strain on the electrochemical and stress corrosion cracking behavior of E690 steel in simulated marine atmosphere. Ocean Engineering, 2019, 182, 188-195.	4.3	26
57	Influence of different heat-affected zone microstructures on the stress corrosion behavior and mechanism of high-strength low-alloy steel in a sulfurated marine atmosphere. Materials Science & Engineering A: Structural Materials: Properties, Microstructure and Processing, 2019, 759, 124-141.	5.6	77
58	Effect of Dissolved Oxygen Concentration on the Microbiologically Influenced Corrosion of Q235 Carbon Steel by Halophilic Archaeon Natronorubrum tibetense. Frontiers in Microbiology, 2019, 10, 844.	3.5	22
59	Influence of graphene oxide on the antiwear and antifriction performance of MAO coating fabricated on Mg Li alloy. Surface and Coatings Technology, 2019, 364, 144-156.	4.8	44
60	Fractal characteristics of AC corrosion morphology of X80 pipeline steel in coastal soil solution. Anti-Corrosion Methods and Materials, 2019, 66, 868-878.	1.5	1
61	Corrosion behavior of X80 pipeline steel in the presence of Brevibacterium halotolerans in Beijing soil. Bioelectrochemistry, 2019, 126, 121-129.	4.6	22
62	Mussel-inspired superhydrophilic surface with enhanced antimicrobial properties under immersed and atmospheric conditions. Applied Surface Science, 2019, 465, 267-278.	6.1	42
63	Corrosion effect of Bacillus cereus on X80 pipeline steel in a Beijing soil environment. Bioelectrochemistry, 2018, 121, 18-26.	4.6	53
64	Effects of cathodic polarization on corrosion fatigue life of E690 steel in simulated seawater. International Journal of Fatigue, 2018, 110, 105-114.	5.7	52
65	Electrochemical characterization and stress corrosion cracking of E690 high strength steel in wet-dry cyclic marine environments. Materials Science & Engineering A: Structural Materials: Properties, Microstructure and Processing, 2018, 710, 318-328.	5.6	106
66	The Effect of Flowing Velocity and Impact Angle on the Fluid-Accelerated Corrosion of X65 Pipeline Steel in a Wet Gas Environment Containing CO2. Journal of Materials Engineering and Performance, 2018, 27, 6636-6647.	2.5	8
67	Laboratory investigation of microbiologically influenced corrosion of Q235 carbon steel by halophilic archaea Natronorubrum tibetense. Corrosion Science, 2018, 145, 151-161.	6.6	67
68	Effect of microstructure on the corrosion resistance of 2205 duplex stainless steel. Part 2: Electrochemical noise analysis of corrosion behaviors of different microstructures based on wavelet transform. Construction and Building Materials, 2018, 189, 1294-1302.	7.2	25
69	Effect of microstructure on the corrosion resistance of 2205 duplex stainless steel. Part 1: Microstructure evolution during isothermal aging at 850â€Â°C and evaluation of anticorrosion properties by methods of cyclic potentiodynamic polarization and electrochemical impedance tests. Construction and Building Materials. 2018, 189, 1286-1293.	7.2	25
70	Modeling for corrosion fatigue crack initiation life based on corrosion kinetics and equivalent initial flaw size theory. Corrosion Science, 2018, 142, 277-283.	6.6	29
71	Effect of SO2 content on SCC behavior of E690 high-strength steel in SO2-polluted marine atmosphere. Ocean Engineering, 2018, 164, 256-262.	4.3	32
72	Electrochemical and Stress Corrosion Mechanism of Submarine Pipeline in Simulated Seawater in Presence of Different Alternating Current Densities. Materials, 2018, 11, 1074.	2.9	13

#	Article	IF	CITATIONS
73	The Corrosion Behavior of AZ91D Magnesium Alloy in Simulated Haze Aqueous Solution. Materials, 2018, 11, 970.	2.9	20
74	Variation of the Corrosion Behavior Prior to Crack Initiation of E690 Steel Fatigued in Simulated Seawater with Various Cyclic Stress Levels. Journal of Materials Engineering and Performance, 2018, 27, 4921-4931.	2.5	10
75	Effect of alternating current on stress corrosion cracking behavior and mechanism of X80 pipeline steel in near-neutral solution. Journal of Natural Gas Science and Engineering, 2017, 38, 458-465.	4.4	35
76	Field experiment of stress corrosion cracking behavior of high strength pipeline steels in typical soil environments. Construction and Building Materials, 2017, 148, 131-139.	7.2	46
77	Effect of Hydrogen Charging on the Stress Corrosion Behavior of 2205 Duplex Stainless Steel Under 3.5Âwt.% NaCl Thin Electrolyte Layer. Journal of Materials Engineering and Performance, 2017, 26, 2837-2846.	2.5	11
78	Influence of sea mud state on the anodic behavior of Al-Zn-In-Mg-Ti sacrificial anode. Ocean Engineering, 2017, 136, 11-17.	4.3	10
79	Dual-action smart coatings with a self-healing superhydrophobic surface and anti-corrosion properties. Journal of Materials Chemistry A, 2017, 5, 2355-2364.	10.3	413
80	Corrosion fatigue crack initiation and initial propagation mechanism of E690 steel in simulated seawater. Materials Science & Engineering A: Structural Materials: Properties, Microstructure and Processing, 2017, 708, 181-192.	5.6	94
81	Effect of pH and hydrogen on the stress corrosion cracking behavior of duplex stainless steel in marine atmosphere environment. Ocean Engineering, 2017, 146, 311-323.	4.3	38
82	Stress corrosion cracking behavior of ZK60 magnesium alloy under different conditions. International Journal of Hydrogen Energy, 2017, 42, 26162-26174.	7.1	50
83	The cost of corrosion in China. Npj Materials Degradation, 2017, 1, .	5.8	652
84	A new understanding of the failure of waterborne acrylic coatings. RSC Advances, 2017, 7, 38135-38148.	3.6	12
85	Effect of negative half-wave alternating current on stress corrosion cracking behavior and mechanism of X80 pipeline steel in near-neutral solution. Construction and Building Materials, 2017, 154, 580-589.	7.2	31
86	Mussel-inspired superhydrophobic surfaces with enhanced corrosion resistance and dual-action antibacterial properties. Materials Science and Engineering C, 2017, 80, 566-577.	7.3	66
87	Failure Mechanisms of the Coating/Metal Interface in Waterborne Coatings: The Effect of Bonding. Materials, 2017, 10, 397.	2.9	28
88	Effect of Zinc Phosphate on the Corrosion Behavior of Waterborne Acrylic Coating/Metal Interface. Materials, 2017, 10, 654.	2.9	28
89	Corrosion Behavior of X80 Steel with Coupled Coating Defects under Alternating Current Interference in Alkaline Environment. Materials, 2017, 10, 720.	2.9	11
90	Effect of Alternating Current on the Cathodic Protection and Interface Structure of X80 Steel. Materials, 2017, 10, 851.	2.9	27

#	Article	IF	CITATIONS
91	Preparation of Superhydrophobic Film on Ti Substrate and Its Anticorrosion Property. Materials, 2017, 10, 628.	2.9	19
92	A Modelling Study for Predicting Life of Downhole Tubes Considering Service Environmental Parameters and Stress. Materials, 2016, 9, 741.	2.9	3
93	Erosion–corrosion behavior of 2205 duplex stainless steel in wet gas environments. Journal of Natural Gas Science and Engineering, 2016, 35, 928-934.	4.4	19
94	Effect of plastic deformation on the electrochemical and stress corrosion cracking behavior of X70 steel in near-neutral pH environment. Materials Science & Engineering A: Structural Materials: Properties, Microstructure and Processing, 2016, 677, 259-273.	5.6	116
95	Electrochemical Behavior and Stress Corrosion Sensitivity of X70 Steel Under Disbonded Coatings in Korla Soil Solution. Journal of Materials Engineering and Performance, 2016, 25, 4657-4665.	2.5	10
96	Comparative study of the SCC behavior of E690 steel and simulated HAZ microstructures in a SO2-polluted marine atmosphere. Materials Science & Engineering A: Structural Materials: Properties, Microstructure and Processing, 2016, 650, 93-101.	5.6	50
97	Effect of hydrogen-induced plasticity on the stress corrosion cracking of X70 pipeline steel in simulated soil environments. Materials Science & Engineering A: Structural Materials: Properties, Microstructure and Processing, 2016, 658, 348-354.	5.6	93
98	The effect of hydrogen on stress corrosion behavior of X65 steel welded joint in simulated deep sea environment. Ocean Engineering, 2016, 114, 216-223.	4.3	52
99	Failure analysis of P110 steel tubing in low-temperature annular environment of CO2 flooding wells. Engineering Failure Analysis, 2016, 60, 296-306.	4.0	25
100	Materials science: Share corrosion data. Nature, 2015, 527, 441-442.	27.8	557
101	Effect of cathodic potentials on the SCC behavior of E690 steel in simulated seawater. Materials Science & Engineering A: Structural Materials: Properties, Microstructure and Processing, 2015, 642, 22-31.	5.6	105
102	Field corrosion characterization of soil corrosion of X70 pipeline steel in a red clay soil. Progress in Natural Science: Materials International, 2015, 25, 242-250.	4.4	34
103	Stress corrosion cracking of E690 steel as a welded joint in a simulated marine atmosphere containing sulphur dioxide. Corrosion Science, 2015, 100, 627-641.	6.6	123
104	Stress Corrosion Cracking of X80 Pipeline Steel Under Various Alternating Current Frequencies in High-pH Carbonate/Bicarbonate Solution. Corrosion, 2014, 70, 1181-1188.	1.1	13
105	In situ corrosion characterization of simulated weld heat affected zone on API X80 pipeline steel. Corrosion Science, 2014, 85, 401-410.	6.6	99
106	Effect of Strength and Microstructure on Stress Corrosion Cracking Behavior and Mechanism of X80 Pipeline Steel in High pH Carbonate/Bicarbonate Solution. Journal of Materials Engineering and Performance, 2014, 23, 1358-1365.	2.5	23
107	Effect of AC current density on stress corrosion cracking behavior of X80 pipeline steel in high pH carbonate/bicarbonate solution. Electrochimica Acta, 2014, 117, 351-359.	5.2	89
108	Mechanistic Aspect of Non-Steady Electrochemical Characteristic During Stress Corrosion Cracking of an X70 Pipeline Steel in Simulated Underground Water. Corrosion, 2014, 70, 678-685.	1.1	43

#	Article	IF	CITATIONS
109	Effect of alternating voltage on corrosion of X80 and X100 steels in a chloride containing solution – Investigated by AC voltammetry technique. Corrosion Science, 2014, 86, 213-222.	6.6	43
110	Effect of AC on stress corrosion cracking behavior and mechanism of X80 pipeline steel in carbonate/bicarbonate solution. Corrosion Science, 2014, 87, 224-232.	6.6	71
111	Effect of pH value on stress corrosion cracking of X70 pipeline steel in acidic soil environment. Acta Metallurgica Sinica (English Letters), 2013, 26, 489-496.	2.9	26
112	Characterization of corrosion products formed on the surface of carbon steel by Raman spectroscopy. Journal of Raman Spectroscopy, 2009, 40, 76-79.	2.5	53
113	Raman and IR spectroscopy study of corrosion products on the surface of the hotâ€dip galvanized steel with alkaline mud adhesion. Journal of Raman Spectroscopy, 2009, 40, 656-660.	2.5	12
114	Effects of cathodic potential on the local electrochemical environment under a disbonded coating. Journal of Applied Electrochemistry, 2009, 39, 697-704.	2.9	17
115	Effects of Microstructure on Corrosion of X70 Pipe Steel in an Alkaline Soil. Journal of Materials Engineering and Performance, 2009, 18, 216-220.	2.5	77
116	Corrosion and Stress Corrosion Cracking Behavior of X70 Pipeline Steel in a CO2-Containing Solution. Journal of Materials Engineering and Performance, 2009, 18, 319-323.	2.5	33
117	Stress corrosion cracking of X80 pipeline steel in simulated alkaline soil solution. Materials & Design, 2009, 30, 1712-1717.	5.1	102
118	Effect of applied potentials on stress corrosion cracking of X70 pipeline steel in alkali solution. Materials & Design, 2009, 30, 2259-2263.	5.1	34
119	Effect of inclusions on initiation of stress corrosion cracks in X70 pipeline steel in an acidic soil environment. Corrosion Science, 2009, 51, 895-900.	6.6	143
120	Effect of cathodic protection on corrosion of pipeline steel under disbonded coating. Corrosion Science, 2009, 51, 2242-2245.	6.6	131
121	Local additional potential model for effect of strain rate on SCC of pipeline steel in an acidic soil solution. Corrosion Science, 2009, 51, 2863-2871.	6.6	121
122	Relationship between electrochemical characteristics and SCC of X70 pipeline steel in an acidic soil simulated solution. Acta Metallurgica Sinica (English Letters), 2009, 22, 58-64.	2.9	31
123	Corrosion resistance of 316L stainless steel in acetic acid by EIS and Mott-Schottky. Journal Wuhan University of Technology, Materials Science Edition, 2008, 23, 574-578.	1.0	8
124	Stress corrosion cracking behavior of X70 pipe steel in an acidic soil environment. Corrosion Science, 2008, 50, 2251-2257.	6.6	178
125	Effect of Alternating Current and Cathodic Protection on Corrosion of X80 Steel in Alkaline Soil. Journal of Materials Engineering and Performance, 0, , 1.	2.5	3